INTERNATIONAL JOURNAL FOR NUMERICAL METHODS IN FLUIDS, VOL. 2, 61–88 (1982)

NUMERICAL PREDICTIONS OF THE LAMINAR FLOW OVER A NORMAL FLAT PLATE

I. P. CASTRO

Department of Mechanical Engineering, University of Surrey, Guildford, England

K. A. CLIFFE AND M. J. NORGETT

Theoretical Physics Division, AERE Harwell, Oxon, England

SUMMARY

Finite-difference and finite-element techniques have been used to calculate the steady laminar flow over a flat plate normal to an air stream, up to a Reynolds number, Re, based on the plate half-width, of 100. The boundary conditions simulate a central splitter plate downstream of the body, to prevent vortex shedding, so the flow is characterized by a closed recirculation region which grows with increasing Re but at $\mathrm{Re} = O(100)$ is very similar in size to the turbulent recirculating region that occurs in the corresponding high Reynolds-number flow. Motivation came, in part, from the increasing efforts of turbulence modellers to calculate complex turbulent flows (containing elliptic regions) and our belief that the numerical methods commonly employed for such work can be inaccurate. The predictions are compared with each other and with some expectations based on classic solutions of the Navier–Stokes equations, and the nature of the numerical errors is demonstrated. It is concluded that effort comparable with that expended in developing turbulence models should be directed to developing higher-order numerical methods, before the numerical accuracy of predictions of, for example, bluff-body flows can be made sufficiently high to sustain detailed discussion of the adequacy of turbulence models in such situations.

KEY WORDS Vector Differencing Finite Element Scheme Recirculating Laminar Flow False Diffusion Conservation of Energy

1. INTRODUCTION

Most of the current understanding of incompressible flow around bluff bodies derives from a vast number and variety of experimental studies carried out over a long period. However, some workers are now attempting, by the use of various increasingly sophisticated turbulence models, to predict bluff-body flows, for which Prandtl's boundary-layer approximation is not valid. For example, Pope and Whitelaw[1] have used several turbulence models to calculate wake flows behind various obstacles, one of which was an axisymmetric disc normal to a free stream. More recently, further studies were reported at the Second Turbulent Shear-Flows Conference[2] and one of the 'set-piece' exercises for the 1980/1 Stanford Conference on Complex Flows was flow past a backward-facing step.

The accuracy of such predictions (which, thus far have all been '*post*-dictions') is limited not only by the validity of the particular turbulence models, but also by the accuracy of the numerical methods used to solve the appropriate equation set. The numerical methods suitable for parabolic, as indeed for hyperbolic, flows can usually be made as accurate as required; most turbulence models have therefore been developed by studying their behaviour in just such applications. However, it is much more difficult to solve the elliptic

0271–2091/82/010061–28$02.80

Received 7 April 1981
Revised 3 July 1981

problems that are encountered in studies of complex flow. Leonard *et al.*[3] have demonstrated convincingly that a variation in the turbulence model can lead to changes in the flow which depend on the method used to discretize the equations. In particular, they found that a high-order difference scheme was necessary if the flow pattern was to reflect faithfully the changes in the turbulence model. In contrast, the well-known hybrid scheme[4,5] which is widely used in turbulence studies, was not satisfactory except when the grid was extensively refined.

It is therefore difficult to separate the consequences of bad physics and bad numerics and, in order to investigate the latter, there are obvious advantages in studying the behaviour of the numerical schemes for laminar flows. However, since the relative magnitude of the various terms in the equations of motion can then be very different—indeed, some terms do not of course appear at all—it is most important to choose flows in which numerical errors are likely to be representative of those that will occur in the fully turbulent cases.

The general character of the various numerical methods available to solve flow equations has of course been deduced principally from studies of simpler model equations which mimic the Navier–Stokes equations (see, for example, Hirt,[6] Cheng,[7] Roache[8]). However, such studies cannot provide a clear guide to the accuracy of particular engineering calculations and can sometimes in fact be misleading. The only convincing test is to compare numerical results with experimental data or analytic flow solutions. A less definitive, but also less demanding test is to compare the predictions of different numerical methods.

In this paper we present a detailed comparison of predictions, obtained using finite-difference and finite-element methods, of a carefully chosen laminar flow. Hutton[9] has recently made a similar comparison based on predictions of flow over a backward-facing step, but for reasons which will become apparent, that is a much less severe test of the numerical techniques. We have chosen to study the steady laminar flow over a two-dimensional flat plate normal to a free stream, with a central splitter plate behind to prevent vortex shedding. There are, unfortunately, very few quantitative experimental data for flow over sharp-edged bodies, but choice of such a flow avoids the well-known difficulty of locating the point of separation on a surface of finite curvature, and also, of course, reduces the co-ordinate-gridding problems to a minimum. Our calculations are therefore truly predictive and we hope to see experimental data compared with them in due course!

Two finite-difference (FD) schemes have been used to represent the steady-state equations; they were solved iteratively (time-marching methods to achieve a steady state are subject to analogous numerical error[8]). The hybrid-differencing scheme (HDS), proposed by Spalding,[4] was selected principally because it is a method which is widely used by engineers, and our second scheme is a generalization of the method originally suggested by Raithby[10] and further studied and developed by Castro[11] and Lillington.[12] This has become known as the vector-differencing scheme (VDS) and, by recognizing that good accuracy requires that the co-ordinate grid should be aligned with the local flow direction in regions of strong cross-flow gradients of the dependent variables, it takes explicit account of the local flow angle. It is therefore a higher-order scheme although, it must be emphasized, not the only possible one. In view of the increasingly evident limitations of HDS (clearly delineated by, for example, Leonard[13] and Gresho and Lee[14] we anticipated that solutions obtained with VDS would be significantly more accurate than those obtained using HDS.

The finite element (FE) scheme we have used was originally introduced by Taylor and Hood[15,16] and has been widely applied in solving problems of laminar fluid flow. It has been employed, for example, in the calculation of channel-entrance problems,[17,18] separated flow over a downstream-facing step,[19] flow in a cavity with a moving lid[20] and separated flow in a pipe expansion.[21] Some of its theoretical properties have recently been analysed by Bercovier and Pironneau[22] and LeTallec.[23]

It is a Galerkin scheme and is, therefore, in some degree equivalent to a central-difference scheme; in consequence, it should provide more accurate solutions for our problem than the finite-difference methods, but requires resolution of the boundary-layer regions of the flow in order to maintain stability.

We do not claim that these schemes are in any way the 'best' for this particular problem. They merely typify those methods in most common use; HDS, in particular, is the method already chosen for some predictions of complex turbulent flows (e.g. McGuirk and Rodi[24]).

Section 2 begins by outlining the general features of the problem to be solved. We expect that some features of the flow, at sufficiently high Reynolds numbers, will be similar to some classic analytic solutions; these expectations are also discussed in Section 2. Section 3 presents the salient features of the three numerical techniques and Section 4 describes the results of the predictions, comparing them with each other and with the expected behaviour of the flow.

It should be emphasized that, whilst the present work concentrates on a laminar flow, we believe that the general conclusions must be valid for the equivalent turbulent flow or, indeed, for any proposed calculations of bluff-body flows using numerical techniques similar to those considered here; indeed, we deliberately chose the particular flow studied in this paper to ensure that this was so. Our specific reasons for this belief are discussed in the concluding section, where it is also argued that there are likely to be further difficulties (additional to those evident from this work) in achieving numerically accurate solutions for turbulent flows. We do not subscribe to the view that, since turbulent eddy viscosities are generally orders of magnitude larger than the laminar viscosity, numerical errors (at least of the 'numerical-viscosity' type) are much less serious in calculations of elliptic turbulent flows.

2. THE PROBLEM

2.1. *The flow considered*

Figure 1 is a sketch of the flow geometry and also gives details of the boundary conditions used in our calculations. Although there are at present no relevant experimental data, we chose an upper boundary condition and blockage ratio, h/D, which could easily be satisfied in, for example, a towing-tank experiment. It is anyway helpful to keep h/D relatively small

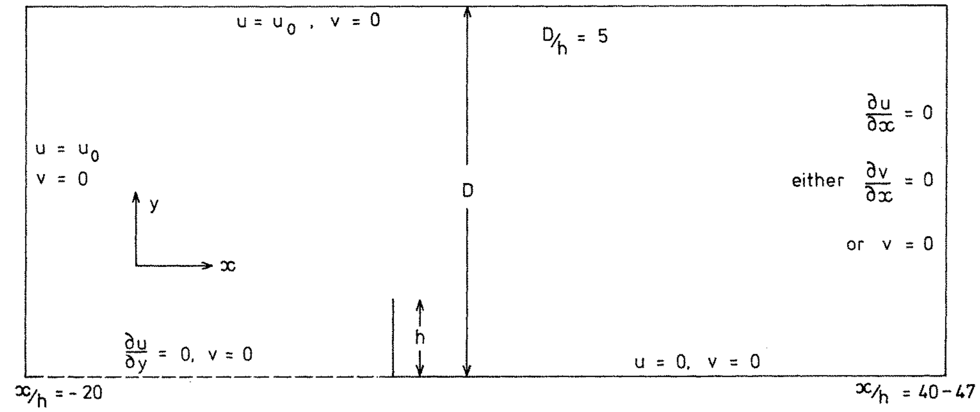

Figure 1. Flow geometry (not to scale) and boundary conditions used for the calculations

since this reduces gridding problems in the vertical, y direction. Note that the lower boundary at $y=0$ upstream of the plate is an axis of symmetry; it is not a solid surface, so the only separation point in the flow is fixed at the fence tip at all values of the Reynolds number.

We have used all three numerical methods for calculations with $10 \leq \mathrm{Re} \leq 100$, where $\mathrm{Re}=u_0h/\nu$ and ν is the kinematic viscosity. It was found (see Section 4) that the distance, L, to reattachment of the separated shear layer for $\mathrm{Re} \approx 70$ was about the same as it is in the high Reynolds-number limit; Arie and Rouse[25] found L/h to be about 18 for $\mathrm{Re}=O(10^5)$. We would therefore expect in the latter case that the turbulent Reynolds number u_0h/ν_e, where ν_e is an eddy viscosity, will be $O(100)$ in the separated, turbulent shear layer behind the plate. More recent measurements in such shear layers confirm this[26] and the implications of this for calculations of the high Reynolds-number turbulent case are discussed in Section 5.

2.2. *Flow near the stagnation point*

If the Reynolds number is small enough, so that the thickness, δ, of the viscous boundary layer on the upstream face of the plate is small compared to the plate width, then the flow around the stagnation point will resemble the classic analytic solution for stagnation flow towards an infinite boundary. This solution is found in standard texts (e.g. Schlichting[27]); in terms of the co-ordinates used in Figure 1, this solution has

$$v=kyf'(\zeta), \qquad u=(\nu k)^{1/2}f(\zeta), \qquad \zeta=-(k/\nu)^{1/2}x; \tag{1}$$

the function $f(\zeta)$ satisfies

$$f'''+f\,.\,f''-f'^2+1=0, \tag{2}$$

where primes denote differentiation with respect to ζ; k is a constant that specifies the surrounding region of inviscid flow where

$$v=ky, \qquad u=-kx. \tag{3}$$

There is a very simple asymptotic solution at large ζ:

$$f(\zeta)=\zeta-0{\cdot}65 \tag{4}$$

If this equation is written in terms of appropriate non-dimensional parameters, then

$$(x/h)k'+0{\cdot}65(k'/\mathrm{Re})^{1/2}+u/u_0=0, \tag{5}$$

where

$$k'=kh/u_0.$$

An analysis of flow along the stagnation streamline leads to an interesting result. A single integration of the u-momentum equation with respect to x yields

$$\Delta H=\frac{\Delta(\frac{1}{2}\rho(u^2+v^2)+p)}{\frac{1}{2}\rho u_0^2}=\frac{2\nu}{u_0^2}\frac{\partial u}{\partial x}\bigg|_1^2+\frac{2\nu}{u_0^2}\int_1^2\frac{\partial^2 u}{\partial y^2}\,\mathrm{d}x; \tag{6}$$

where ΔH is the change in total head between points 1 and 2, expressed in non-dimensional form after division by $\frac{1}{2}\rho u_0^2$, and ρ is the fluid density.

Now, since:

(i) the flow outside the viscous boundary layer is irrotational;

(ii) $\left.\dfrac{\partial u}{\partial x}\right|_{x=0} = 0$;

(iii) $\left.\dfrac{\partial u}{\partial x}\right|_{x=x_\nu} = -k$, where x_ν marks the edge of the boundary layer;

(iv) $u \neq f(y)$ for $x_\nu < x < 0$

it is evident that the rise in total head is given by $2k'/\mathrm{Re}$ and that this increase occurs entirely within the boundary layer. This result applies for both a finite and an infinite plate: but in the latter case the contribution to ΔH comes entirely from the first term in equation (6); while for a finite plate, if the lower limit of integration is sufficiently far upstream so that $\partial u/\partial x = 0$, then the value of $\Delta H = 2k'/\mathrm{Re}$ is the same, but only the second term contributes. Thus for a finite plate the value of k' is not arbitrary, as it is in some sense for an infinite body; k' is fixed by the potential flow surrounding the body and therefore by the body shape, since it is this that determines the variation in the velocity field outside the viscous boundary layer.

We can deduce the appropriate value of k' from the numerical results by plotting u/u_0 against x/h for the region just outside the viscous boundary layer; we then compare the calculated values through the viscous region with the analytic solutions defined by equations (1) and (2). Since $\delta/h = O(\mathrm{Re}^{-1/2})$, we would certainly expect the flow at $\mathrm{Re} = 100$ to contain a fairly extensive region that satisfies the classic solution; this region should shrink at progressively lower Reynolds numbers. At $\mathrm{Re} = 10$, we might expect very little similarity to the analytic solution even close to the stagnation point.

If the boundary layer remains laminar near the stagnation point, the conclusions as to the value of ΔH remain valid for high Reynolds-number flow, although the wake is certainly fully turbulent; but ΔH is then of course very small and certainly not measurable. It should be noted that in the latter case it would in practice be impossible to define a fine-enough grid to resolve the boundary layer; this point is discussed further in Sections 4 and 5.

2.3. The separated shear layer and recirculating region

For the equivalent high Reynolds-number turbulent flow the separated shear layer has a form similar to a classic plane turbulent mixing layer. Although its detailed turbulence structure is rather different—it is distorted by curvature and, near reattachment, by the presence of a solid boundary[26]—the mixing layer still grows at a rate roughly proportional to x and independent of Re. Similarly, in the present case we would expect the separated shear layer to behave roughly like a classic two-dimensional laminar mixing layer growing between two uniform streams. Like many laminar boundary-layer-type flows, this grows like $(\nu x/u_0)^{1/2}$.[27] At least in the region where the pressure gradients imposed on the layer are small, its thickness, δ_1, is therefore expected to behave like

$$\delta_1/h = \alpha\left(\frac{x/h}{\mathrm{Re}}\right)^{1/2} \tag{7}$$

where α is a constant not too different from that found for a plane laminar mixing layer. Our results are compared on this basis in Section 4.

We employ fairly crude physical arguments to determine how the distance to reattachment, L, and the pressure across the recirculating region (the 'bubble') vary with Reynolds number. Assuming that the shear layer grows like $(\nu x/u_0)^{1/2}$ all the way to reattachment, and since this presumably occurs when the layer's thickness is $O(h)$, we have

$$\delta_R/h \sim \left(\frac{L/h}{\mathrm{Re}}\right)^{1/2} = O(1), \tag{8}$$

where δ_R is the shear-layer thickness at reattachment; thus $L/h \sim \mathrm{Re}$. Although this will clearly not be true for $\mathrm{Re} = O(1)$, it does seem likely that for higher Reynolds numbers the length of the bubble will increase linearly with Re. In the limit of $\mathrm{Re} \to \infty$, the flow contains a vortex sheet emanating from the tip of the fence and trailing downstream to infinity; however in practice, of course, both physically and in any attempted *steady* flow prediction, the shear layer becomes unstable long before this limit is reached.

The lateral forces acting on the bubble must be in equilibrium; if the viscous shear on the lower boundary is negligible, then the pressure difference across the bubble integrated over its height must balance the viscous shear acting at the top of the recirculating zone integrated over its length. The pressure difference can be approximated by the base pressure at the back of the fence, and the viscous shear stress by the stress acting at the centre line of the separated shear layer: then

$$-C_{pb} \, . \, h \approx \int_0^L \mu \frac{u_0}{\delta_l} \, . \, \mathrm{d}x / \tfrac{1}{2}\rho u_0^2, \tag{9}$$

where μ is the dynamic viscosity and C_{pb} the base pressure put into non-dimensional form after division by the upstream dynamic head $\frac{1}{2}\rho u_0^2$. Now because $\delta_l \sim (xh/\mathrm{Re})^{1/2}$, we find $C_{pb} \sim [(L/h)/\mathrm{Re}]^{1/2}$, and hence that the base pressure is independent of Reynolds number because $L/h \sim \mathrm{Re}$. This is not a surprising result as the base pressure is presumably set by the dynamics of the flow near the separation point, just as it is in the high Reynolds-number turbulent case. In Section 4, our numerical predictions are compared with this expected behaviour of L and C_{pb}.

Note finally that errors of the 'numerical-viscosity' type are expected to increase the spreading rate of the separated shear layer and lead to early reattachment. For the HDS scheme such errors, as is well known, increase without limit, in the sense that the effective Reynolds number has an upper bound that depends only on the grid details and not on further increases in Re.

3. THE NUMERICAL TECHNIQUES

The equations governing the steady flow of a Newtonian viscous fluid in a two-dimensional region Ω are the Navier–Stokes equations and the equation of continuity:

$$\begin{aligned} u\frac{\partial u}{\partial x} + v\frac{\partial u}{\partial y} &= -\frac{1}{\rho}\frac{\partial p}{\partial x} + \nu\nabla^2 u, \\ u\frac{\partial v}{\partial x} + v\frac{\partial v}{\partial y} &= -\frac{1}{\rho}\frac{\partial p}{\partial y} + \nu\nabla^2 v, \\ \frac{\partial u}{\partial x} + \frac{\partial v}{\partial y} &= 0; \end{aligned} \tag{10}$$

where u (or v) is the component of velocity in the x (or y) co-ordinate direction, p is the pressure, ρ is the fluid density and ν is the kinematic viscosity.

An appropriate set of boundary conditions has (u, v) specified over part of the boundary

(Γ_D) and ($\mathbf{n}\,.\,\nabla u, \mathbf{n}\,.\,\nabla v$), where $\mathbf{n}$ is the outward-facing unit normal, specified over the rest of the boundary (Γ_N); the entire boundary is $\Gamma = \Gamma_D + \Gamma_N$.

3.1. The finite-difference methods

The majority of workers currently predicting high Reynolds-number elliptic flows use turbulence models which allow each equation to be written in the form

$$\frac{\partial u\psi}{\partial x}+\frac{\partial v\psi}{\partial y}=\frac{\partial}{\partial x}\left(\Gamma_x\frac{\partial\psi}{\partial x}\right)+\frac{\partial}{\partial y}\left(\Gamma_y\frac{\partial\psi}{\partial y}\right)+S_\psi; \tag{11}$$

where ψ is the dependent variable, S_ψ is a source term, and $\Gamma_{x,y}$ are diffusivities. Each of the equations is then solved using the same differencing scheme. In the case of the equation expressing the transport of turbulence energy, k, then ψ would be $k, \Gamma_{x,y}$ would involve a turbulent Prandtl number and S_ψ would contain the production and dissipation terms. It should be noted that, in many regions of a typical flow, S_ψ would be the dominant term in the equation. In a laminar flow, equation (11) represents the momentum equations only, so ψ is u or v, $\Gamma_{x,y}$ is the laminar viscosity and S_ψ is simply the pressure-gradient term. The coupled problems of determining the pressure field and satisfying continuity are dealt with by deriving and solving a pressure perturbation equation, as described by Patankar and Spalding.[27] The momentum equations are then solved with the pressure gradients treated as known sources.

Equation (11) is written in finite-difference form by integrating over finite control volumes, like that shown in Figure 2. Cell boundaries are placed half-way between adjacent nodes, linear variations of the flow parameters are assumed and equation (11) becomes

$$A_P\psi_P=\sum_{J=N,S,E,W}A_J\psi_J+S_\psi, \tag{12}$$

where the A_J coefficients contain convective and diffusive flow rates. Equation (12) is solved for ψ_P everywhere by using a standard alternating-direction implicit (ADI) scheme; details of the whole procedure can be found in the literature (e.g. Gosman *et al.*,[5] Roache[8] and Pope

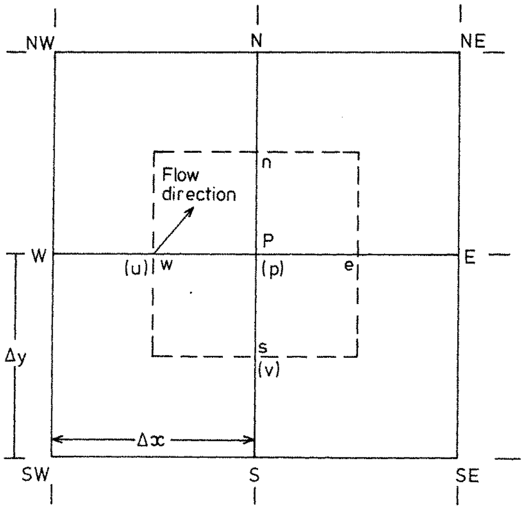

Figure 2. Unit of the finite-difference grid, showing control volume (dashed lines) surrounding point P.

and Whitelaw[1]). it should be noted that, in common with other workers (e.g. Fromm and Harlow,[29] Lilly[30] and Deardoff[31]) and as required in the method for calculating the pressure field, we used a staggered grid with velocities defined at cell boundaries and pressures at cell centres.

It is well known that the finite-difference matrix obtained by central differencing of the convective terms in the flow equations is not diagonally dominant if the mesh Reynolds number $\mathrm{Re_m}$ exceeds two, where $\mathrm{Re_m}$ is defined thus in terms of the grid spacing Δx:

$$\mathrm{Re_m} = u_\mathrm{P} \Delta x / \nu. \tag{13}$$

In this circumstance, the usual methods of solution, typified by ADI, are sometimes unstable and may not converge. This difficulty is often avoided by upwinding the convective terms or, at best, through a hybrid scheme in which central differencing is used where possible ($\mathrm{Re_m} < 2$), and upwind differencing is used elsewhere.[32,4] As indicated previously, it is possible to analyse these finite-difference equivalents of equation (11) analytically, but this has almost always been done for cases where $S_\psi = 0$ and ψ is a *scalar* variable. For a one-dimensional scalar convection–diffusion equation it has been shown many times that upwinding, unlike central differencing, gives the exact solution asymptotically as $\mathrm{Re_m} \rightarrow \infty$. There are, however, first-order error terms which act like extra diffusion and can dominate real diffusion if $\mathrm{Re_m} > 2$; in this case, it is common in the hybrid-differencing scheme to drop the real diffusion terms altogether, which will at least reduce numerical-viscosity errors. The HDS used here follows this procedure. In addition, it has been shown that, in a two-dimensional flow, upwinding can be inaccurate unless the co-ordinate grid is aligned with the flow direction,[33] that even in one dimension upwinding can be inaccurate at large $\mathrm{Re_m}$ if the equation is non-linear,[34] and that the presence of significant source terms can alter the whole behavior of the differencing scheme.[12]

The standard hybrid-differencing scheme was consequently not expected to give accurate results for the present flow at the higher Reynolds numbers. As mentioned earlier, we have therefore also used a vector-differencing scheme (VDS), which is in fact a modification of the scheme proposed by Raithby.[10] In this scheme, if $\mathrm{Re_m}$ exceeds two, the value of u in the u-momentum equation at, for example, the west boundary of the cell (this is written u_w and is to be distinguished from u_W which is the value of u at the adjacent node, see Figure 2) is calculated by interpolation between u values at surrounding nodes, with interpolation always in an upwind sense. Thus the interpolation scheme depends explicitly on the flow angle, $\tan^{-1}(v_\mathrm{w}/u_\mathrm{w})$, with an interpolation made between u_W and u_SW if $v_\mathrm{w}/u_\mathrm{w} < 2\Delta y/\Delta x$; otherwise, with u and v both positive as in Figure 2, the interpolation is between u_SW and u_S. This procedure distinguishes the present scheme from that used by Raithby[10] who put $u_\mathrm{w} = u_\mathrm{SW}$ if $v_\mathrm{w}/u_\mathrm{w} > 2\Delta y/\Delta x$.

This scheme introduces additional terms like $A_\mathrm{SW} u_\mathrm{SW}$ into the right hand side of equation (12). For each node P there are at most only an extra two terms, but over the whole flow field all four extra nodes may be used, so that the difference matrix may be significantly wider-banded. Furthermore, although diagonal dominance is no longer assured, the difference matrix for $\mathrm{Re_m} > 2$ is in general much closer to diagonal dominance than is the central-difference matrix (possible instabilities are, in fact, bounded). In the present work all these extra terms are placed in the 'known' source term, S_u, so previous values for u_SW, etc. are used. This enhances the stability of the scheme and allowed us to use the same ADI-solution algorithm that was used with the HDS method. In view of studies of the accuracy of schemes like this for two-dimensional scalar equations,[10–12] we anticipated some improvement of accuracy, particularly in (and consequently downstream of) regions where transverse velocities were of the same order as axial velocities. We did not, however, expect much improvement in regions where $u \gg v$ and $\mathrm{Re}_m \gg 2$ since the scheme then reduces to HDS. Alternative higher-order methods, like the scheme recently suggested by Leonard,[35] or the 'source-correction' modification to VDS proposed by Lillington,[12] may be rather better in such regions.

3.2. The finite-element method

The natural description of the finite-element method is in terms of various function spaces. We write $H'(\Omega)$ to represent the space of all functions whose derivatives are square-integrable over Ω, and $H'_\mathrm{D}(\Omega)$ is the more restricted space of all functions which belong to $H'(\Omega)$ and are zero on Γ_D. The starting point for the finite-element discretization is a weak form of the flow equations (10) and the boundary conditions. We introduce $\hat{u}$ and $\hat{v}$ that belong to $H'(\Omega)$ and satisfy the boundary conditions on Γ_D. The weak formulation of the Navier–Stokes and continuity equations that we employ is:

find (u, v, p) such that

$$u - \hat{v} \text{ belongs to } H'_\mathrm{D}(\Omega);$$
$$u - \hat{v} \text{ belongs to } H'_\mathrm{D}(\Omega);$$
$$p \text{ belongs to } H'(\Omega);$$

and

$$\begin{aligned}
&\int_\Omega \left(u\frac{\partial u}{\partial x}+v\frac{\partial u}{\partial y}+\frac{1}{\rho}\frac{\partial p}{\partial x}\right)w\,\mathrm{d}\Omega+\nu\int_\Omega \nabla u\,.\,\nabla w\,\mathrm{d}\Omega=\int_{\Gamma_\mathrm{N}} f_u w\,\mathrm{d}\Gamma, \quad \text{for all } w \text{ in } H'_\mathrm{D}(\Omega),\\
&\int_\Omega \left(u\frac{\partial v}{\partial x}+v\frac{\partial v}{\partial y}+\frac{1}{\rho}\frac{\partial p}{\partial y}\right)w\,\mathrm{d}\Omega+\nu\int_\Omega \nabla v\,.\,\nabla w\,\mathrm{d}\Omega=\int_{\Gamma_\mathrm{N}} f_v w\,\mathrm{d}\Gamma, \quad \text{for all } w \text{ in } H'_\mathrm{D}(\Omega),\\
&\int_\Omega \left(\frac{\partial u}{\partial x}+\frac{\partial v}{\partial y}\right)q\,\mathrm{d}\Omega=0, \quad \text{for all } q \text{ in } H'(\Omega);
\end{aligned} \tag{14}$$

where f_u (or f_v) is the value of $\mathbf{n}\,.\,\nabla u$ (or $\mathbf{n}\,.\,\nabla v$) on Γ_N, and w and q are test functions.

It is easy to see that a classical solution (that is a solution having continuous derivatives of all orders appearing in the equations) is also a weak solution, and that any weak solution that has sufficient continuity is a classical solution. It should be noted, however, that the weak form also allows less smooth solutions, and it therefore is a generalization of the classical form.

An approximate solution of the flow equations is obtained by requiring that the flow fields belong to particular finite-element spaces of limited dimension. The functions in the finite-element spaces $W^h(\Omega)$ and $Q^h(\Omega)$ also have square-integrable first derivatives, and such functions that in addition are zero at the boundary are members of $W^h_\mathrm{D}(\Omega)$. The superscript h is some measure of the element size, and also of the dimension of the function spaces, so that any function in $H'(\Omega)$ can be approximated with arbitrary accuracy by a member of a finite-element space for sufficiently small h.

If $\hat{u}^h$ and $\hat{v}^h$ belong to $W^h(\Omega)$, and approximately satisfy the boundary conditions on Γ_D, then the finite-element representation of the flow is obtained thus from the flow equations in weak form:

find (u^h, v^h, p^h) such that

$$u^h - \hat{v}^h \text{ belongs to } W^h_D(\Omega),$$
$$v^h - \hat{v}^h \text{ belongs to } W^h_D(\Omega),$$
$$p^h \text{ belongs to } Q^h(\Omega);$$

and the equations of (14) are satisfied with u^h, v^h, $\hat{u}^h$, $\hat{v}^h$, p^h, w^h and q^h replacing $u, v, \hat{u}, \hat{v}, p, w$ and q. The trial functions u^h, v^h and p^h are determined if the weak forms of the flow equations are satisfied exactly for a sufficient number of test functions w^h and q^h. In the Galerkin method, these test functions span the spaces $W^h_D(\Omega)$ and $Q^h(\Omega)$. We note that it is not possible to choose these spaces arbitrarily,[36,37]; indeed this is why the formulation is necessarily in terms of separate finite-element function spaces for the velocity and pressure fields. An injudicious choice of these distinct spaces leads to equations that do not determine the pressure uniquely.

Such finite-element spaces have been discussed many times (see for example Zienkiewicz,[38]), so we give only a brief description of our own method of calculation. The region Ω was divided into quadrilaterals, which are related through an isoparametric mapping to a basic rectangular element. Each such element has nine nodes (see Figure 3), and a basis function is associated with each node which has value one at that node but is zero at all other nodes. Each basis function is a biquadratic function of the co-ordinates over each rectangle so that it is non-zero only on those elements that contain the particular node. This set of functions provides a basis for the finite-element space $W^h(\Omega)$, and $W^h_D(\Omega)$ is obtained by omitting those functions associated with nodes on the boundary Γ_D; the velocity fields are sought within these spaces. A basis for the pressure space $Q^h(\Omega)$ is obtained using the same elements; however, we now associate basis functions only with the vertex nodes and the functions are bilinear in the co-ordinates. This combination of approximations leads to a pressure field that is unique up to a constant. In fact, it has been shown that, with suitable restrictions on the problem, this particular approximation converges to the solution of the Navier–Stokes equations as $h \to 0$.[22,23]

This procedure leads to a set of non-linear equations for the nodal values, which is solved

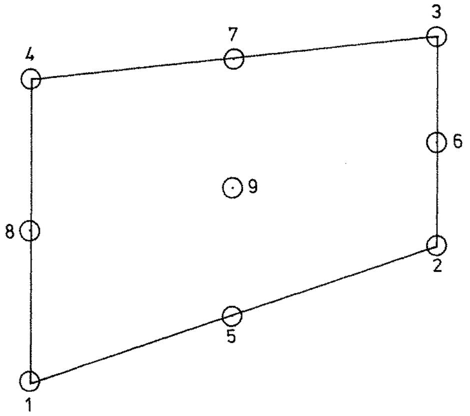

Figure 3. Basic nine-noded-quadrilateral finite element, with basis functions for the u and v fields at all nodes and functions for p defined at nodes 1 to 4

by a Newton–Raphson algorithm. The linear system of equations produced at each iteration is solved using the frontal method.[39]

Although the finite-element approximation is derived in a very different way, it has features in common with central-difference approximations. In particular, the leading-order truncation error is proportional to the third derivative of the velocity. This leads to oscillating solutions when the mesh Reynolds number exceeds two in regions where the variables are changing rapidly. Thus, in order to obtain oscillation-free solutions, it is usually necessary to resolve the boundary layers present in the flow.[14] The other feature of the method is that the approximation of the convective terms is such as to 'almost conserve' the total head $(\frac{1}{2}\rho(u^2+v^2)+p)$ of the fluid in regions of irrotational flow (there is a small error because the continuity equation is only approximately satisfied). This is in contrast to the finite-difference schemes described in the previous section, which do not have this property; the consequences of this are discussed in Section 4.1.

3.3. Boundary conditions and gridding

Calculations of the potential flow about a bluff body suggest that the obstacle has no influence upstream at distances exceeding ten times the body height,[40] the upstream boundary was therefore fixed at $x/h=-20$. The appropriate inlet boundary condition has $u=u_0$ and $v=0$. The downstream boundary was generally placed at $x/h=40$–47, as calculations with x/h increased to 64 showed that the downstream boundary was having no effect on the recirculation region in the shorter channel. The finite-element calculations had Neumann boundary conditions at the outlet with $\partial u/\partial x=0$ and $\partial v/\partial x=0$, but in the finite-difference calculations it was convenient to set $v=0$.

Symmetry conditions were imposed along the stagnation streamline so that $\partial u/\partial y=0$ and $v=0$. A splitter plate extended downstream from the plate so that here both velocity components were set at zero; at the upper boundary, the velocity fields were fixed with $u=u_0$ and $v=0$. Thus all the boundary conditions were close to what could be realized in a towing-tank experiment, which is probably the simplest way of obtaining relevant experimental data.

It is not practicable to cover such an extended region of flow with a uniform grid and yet provide sufficient refinement near the obstacle, particularly at the separation point. In order to obtain good accuracy, we would expect that the grid spacing there must be some small fraction of h. We employed various finite-difference grids to achieve a satisfactory description of the flow, but most results were obtained using one of the three grids specified in Table I. Grid 1, the basic grid used for much of the work, had minimum mesh spacings, $\Delta x/h$ and $\Delta y/h$, around the plate tip of 0·06 and 0·014 respectively; grid 2 had rather more definition in the irrotational region upstream $(x/h \lesssim -2)$; grid 3 had more resolution in the viscous region near the plate itself. All three grids had identical y-node deployment, but other distributions were studied during the course of the work; the influence of such changes in the y-mesh is discussed where relevant.

One of the major advantages of the finite-element method is that it is easier to concentrate grid nodes in appropriate regions without wasting computational effort elsewhere. Table II records the grid used for calculations at $\mathrm{Re}=100$, and Figure 4 illustrates how a finite-element grid can concentrate nodes into regions where the dependent variables have large gradients; in this case, the nodes are deployed beyond the plate to follow the deflection of the centre of the separated shear layer. This grid was also used for some calculations at lower Reynolds number, but for $\mathrm{Re}<100$, we also contracted the grid downstream from the

Table I. Finite-difference grids

y/h	x/h, x<0			x/h, x>0		
Grids 1,2,3	Grid 1	Grid 2	Grid 3	Grid 1	Grid 2	Grid 3
0·0						
0·02	−20·0	−20·0	−20·0	0·03	0·03	0·005
0·06	−17·0	−18·2	−18·0	0·09	0·09	0·019
0·11	−11·0	−14·6	−14·0	0·17	0·17	0·037
0·16	−8·0	−11·8	−10·0	0·27	0·27	0·062
0·22	−6·0	−9·8	−7·11	0·40	0·40	0·097
0·30	−4·4	−8·0	−5·42	0·55	0·55	0·143
0·40	−3·2	−6·6	−4·13	0·75	0·75	0·206
0·50	−2·3	−5·6	−3·14			0·292
0·60	−1·7	−4·8	−2·39			0·41
0·70	−1·3	−4·2	−1·81			0·57
0·78	−1·0	−3·7	−1·38			0·79
0·85		−3·3	−1·04			
0·90		−2·9				
0·93		−2·5				
0·96		−2·1		1·00	1·00	1·08
0·98		−1·7		1·30	1·30	1·48
0·993		−1·3		1·70	1·70	2·02
1·007		−1·0		2·25	2·25	2·76
1·02				3·10	3·10	3·77
1·04				4·2	4·2	5·14
1·07				5·6	5·6	7·0
1·11	−0·75	−0·75	−0·79	7·4	7·4	9·5
1·15	−0·55	−0·55	−0·59	9·6	9·6	12·5
1·19	−0·40	−0·40	−0·44	12·2	12·0	17·0
1·24	−0·27	−0·27	−0·33	15·6	14·7	22·0
1·32	−0·17	−0·17	−0·24	21·0	17·7	28·0
1·42	−0·09	−0·09	−0·175	28·0	21·0	35·0
1·55	−0·03	−0·03	−0·125	36·0	25·0	43·0
1·70			−0·087	40·0	29·7	47·0
1·9			−0·058		35·0	
2·2			−0·035		43·0	
2·6			−0·018		47·0	
3·0			−0·005			
3·5						
4·0						
4·4						
4·7	Grid 1		40×40		(x x y)	
4·9	Grid 2		50×40			
5·0	Grid 3		50×40			

barrier so that nodes were placed at points with the same value of x/Re. This distributes the same number of nodes in the recirculation zone at all values of Re, and leads to an improved description of the growth of the shear layer for smaller values of the Reynolds number.

4. RESULTS AND DISCUSSION

For this study, we have calculated flows at various Reynolds numbers, using many different gridding arrangements for each of the three numerical methods. We cannot of course present all such results, or indeed a full description of any particular prediction; rather we intend, as

Table II. Finite-element grids. This table locates the positions of the corner nodes of the quadilateral elements used to discretize the flow geometry (nodes 1 to 4 in Figure 3). Basis functions for the pressure fields are localized only about these corner nodes; velocity fields are described by basis functions at these points and also by functions centred at the midpoint of the edge of each element and at the element centre

y/h		x/h	
$x\leq 0{\cdot}0$	$x\geq 2{\cdot}54h$	$x\leq 0{\cdot}0$	$x\geq 0{\cdot}0$
0·00	0·00	−20.0	0.0
0·06	0·06	−9·5	0·12
0·16	0·16	−5·2	0·46
0·30	0·30	−2.75	1·08
0·50	0·50	−1·50	1·98
0·70	0·70	−1·00	3·18
0·85	0·88	−0·60	4·68
0·93	1·02	−0·34	6·49
0·98	1·30	−0·20	8·61
1·00	1·60	−0·12	11·03
1·02	1·90	−0·06	13·77
1·07	2·10	−0.025	16·81
1·15	2·25	0·0	20·17
1·24	2·40		23·84
1·42	2·55		27·83
1·70	2·70		32·12
2·2	3·0		36·74
3·0	3·7		41·67
4·0	4·4		47·00
4·7	4·8		
5·0	5·0		

Values of y/h for $0{\cdot}0<x/h<2.54$ are obtained by linear interpolation between values used at the end of this interval. The finite-element grid is 32×20 elements in the x and y directions.

indicated earlier, to pick out the most significant observations and analyse salient features of the results. Now at low Reynolds number the only practicable criteria for establishing the accuracy of a prediction are that the results should be independent of the chosen grid, and that the different numerical methods should lead to similar results. Indeed, we found that it was not difficult to obtain accurate solutions for this type of flow. In contrast, at high Reynolds numbers we can also check numerical results against the analytic predictions set out in Section 2. We have therefore concentrated on analysing results at higher Reynolds number, particularly for $\mathrm{Re}=100$, where we expect that the several numerical methods may well lead to significantly different predictions.

The results are assessed by posing these questions:

(i) At the highest Reynolds number considered ($\mathrm{Re}=100$), how do the predictions differ in the region upstream of the fence where $x\leq 0$? If we achieve a reasonable resolution of the upstream boundary layer, and accurately predict variables along, say, $x=0$, then downstream differences must result from local errors rather than convection of errors generated upstream. (We have shown previously, for a turbulent flow, how errors that arise around a separation corner can be propagated downstream, and thus can confuse identification of the

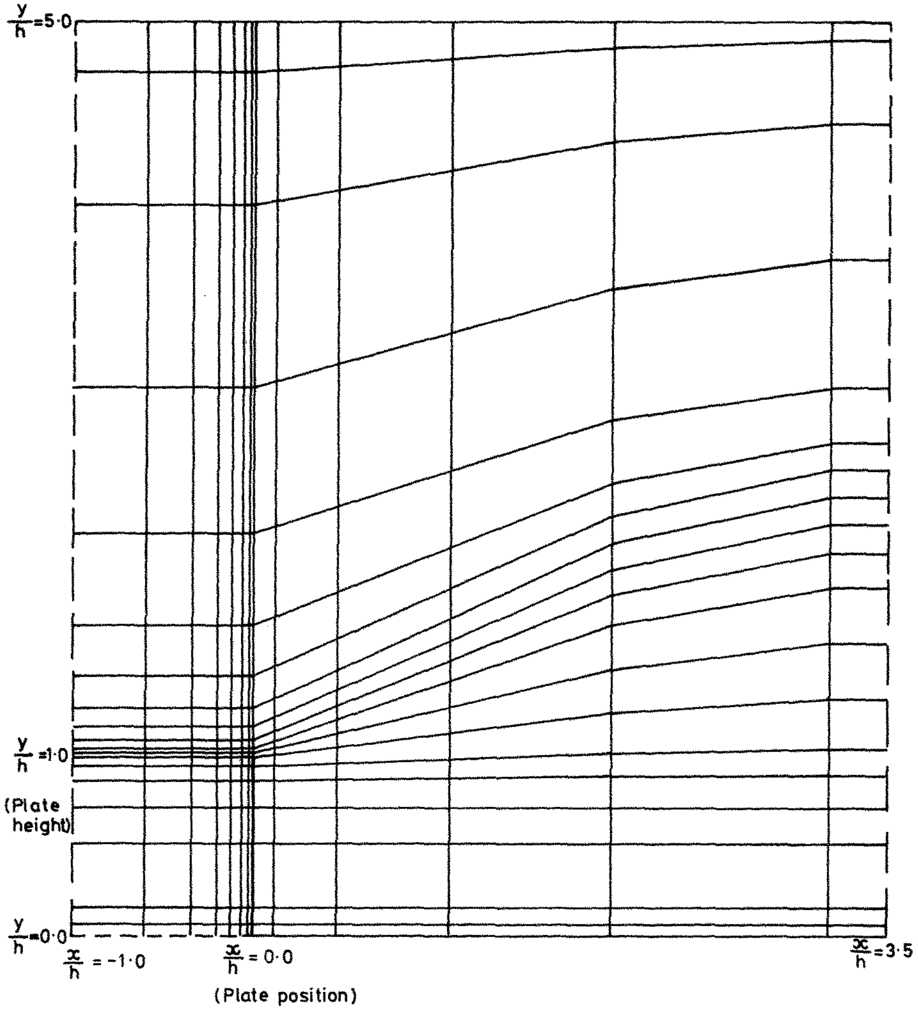

Figure 4. Disposition of finite elements near the plate, showing concentration of elements at the plate tip and on the face of the plate, and the deployment of a high density of elements downstream in the shear layer

source of errors.[34]) We also note that if upstream solutions are accurate for $\mathrm{Re} = 100$, then there is no reason to doubt the numerical accuracy of calculations for lower Reynolds number.

(ii) How do the various numerical solutions differ in their detailed description of flow downstream of the fence: in particular, their prediction of the growth of the shear layer as a function of $(x/\mathrm{Re})^{1/2}$, the increase in length of the recirculation region at large Reynolds number, and the variation in surface pressure?

Subsidiary questions, for example the gridding required for grid-independent solutions, or the effect of downstream boundary conditions, will be addressed as necessary but within this framework.

4.1. *The upstream flow* $(x \leq 0)$

We begin by discussing the numerical errors in calculations for the irrotational region upstream of the viscous boundary layer. Figure 5 shows the change in total head ΔH along

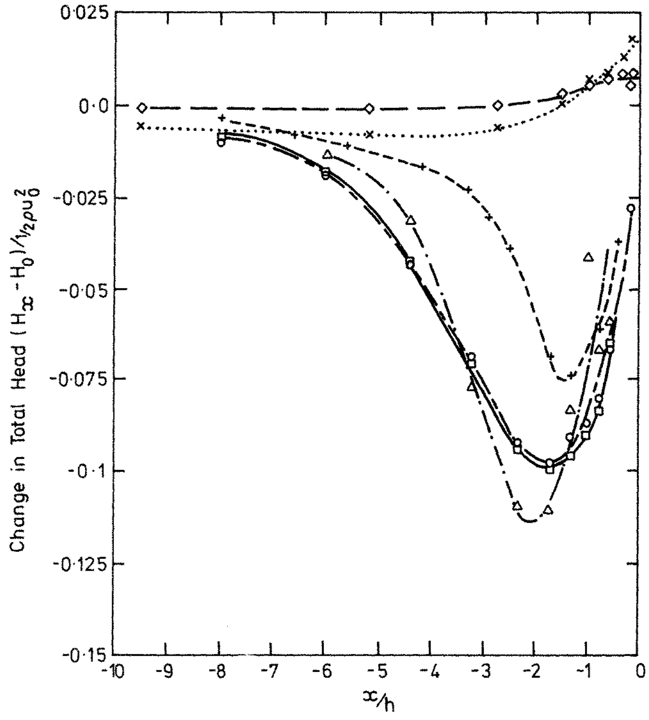

Figure 5. Change in Total Head along the stagnation streamline. VDS, Grid 1, Re = :△, 10; □, 50; ○, 100. VDS, Grid 2, Re = 100; +. FE, Re = :×, 30; ◇, 100

the stagnation streamline ($y = 0$) for two finite-difference and one finite-element simulation at various values of Re. The FD predictions were obtained using the vector scheme (hybrid-scheme results were identical along $y = 0$ because $v = 0$). The sets of x co-ordinates used in the two FD studies and the positions of the FE nodes are given in Tables I and II.

Since we expect that the FE method will conserve energy to good accuracy, it is no surprise to find that the only significant changes in ΔH occur in the viscous region, but the FD results are very different. First, since mesh Reynolds numbers greatly exceed two except very close to the plate, upwinding leads to significant errors; however, such errors are reduced by refining the grid in the region where mesh Reynolds numbers were inevitably large. It is also clear that there is an upper bound on the errors as the Reynolds number is increased: Figure 5 includes predictions (obtained with grid 1) at Re = 10 and Re = 50, and these latter results are almost identical with the predictions for Re = 100. This behaviour is different from that of the scalar convection–diffusion equation, where errors due to upwinding continue to increase with Reynolds number, but it is not unexpected since Castro[34] has found similar behaviour in a comparable study. The explanation is straightforward: along the stagnation streamline the solution of the upwinded finite-difference form of the flow equations must effectively satisfy the equation

$$u\frac{\partial u}{\partial x}+\frac{1}{\rho}\frac{\partial p}{\partial x}=\nu\nabla^2 u+\frac{1}{\rho}\frac{\partial}{\partial x}\left[\tfrac{1}{2}\rho u\Delta x\frac{\partial u}{\partial x}\right]; \qquad (15)$$

where, as usual, the last term represents the numerical diffusion, which depends on the grid spacing Δx. In the irrotational region a single integration leads to

$$\Delta H]_1^2 = \int_1^2 \frac{\partial}{\partial x}\left(\tfrac{1}{2}\rho u \Delta x \frac{\partial u}{\partial x} \mathrm{d}x\right) \Big/ \tfrac{1}{2}\rho u_0^2, \tag{16}$$

and if limit 1 is sufficiently far upstream, then

$$\Delta H = \frac{u}{u_0} \cdot \frac{\partial(u/u_0)}{\partial(x/h)} \cdot \frac{\Delta x}{h}. \tag{17}$$

At large Re, $u/u_0 \neq f(\mathrm{Re})$, so the change in head that arises from the use of upwinded finite differences does not depend on Re; it is greatest where $u\frac{\partial u}{\partial x}$ is largest and decreases with $\Delta x/h$, as the results of Figure 5 demonstrate. Notice that the errors depend only on local conditions, and therefore reduce again as $x \rightarrow 0$. The implications of these errors in the description of the irrotational region, which arise essentially because we must there solve an inviscid flow with a method more suited to viscous flow, will be discussed in Section 5.

If we turn now to the prediction of the viscous boundary layer, Figure 6 shows u and v at Re = 100 expressed as values of the boundary-layer functions $f(\zeta)$ and $f'(\zeta)$ that were defined in Section 2.2. The results were computed using the vector scheme and a grid (grid 3, Table I) similar to grid 1 but refined in the region $-2 \leq x/h \leq 2$. The k' value required to fit the (small) linear u-velocity region [equation (5)] was $k' = 0{\cdot}825$, and it is clear that the expected behaviour is obtained up to $\zeta \simeq 2(x/h \simeq -0{\cdot}18)$ and for $y/h \lesssim 0{\cdot}35$. In this region mesh Reynolds numbers are below two, so that hybrid-scheme results are very similar (central

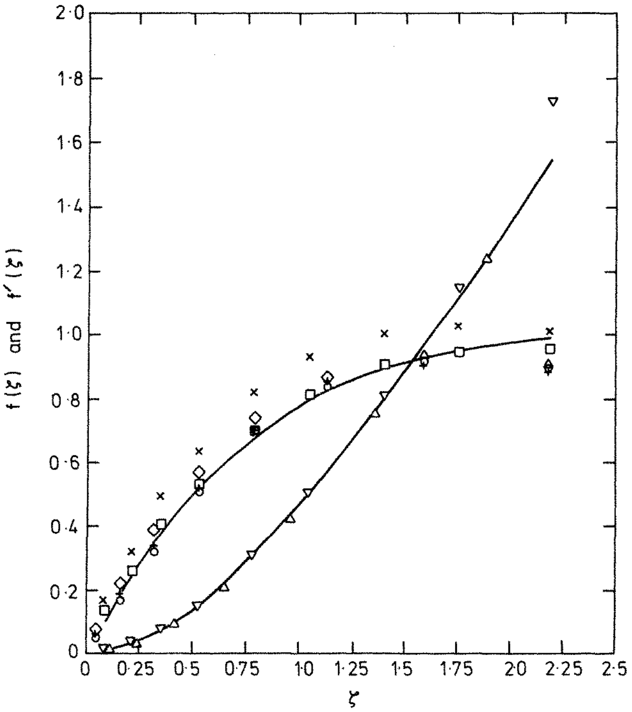

Figure 6. Boundary layer functions. Re = 100. $f(\zeta)$:△, VDS; ▽, Fe. $f'(\zeta)$, VDS, y/h = :○, 0·04; +, 0·35; ◇, 0·55. $f'(\zeta)$, FE, y/h = :□, 0·06; ×, 0·5.———, analytic solution

differencing invoked by both schemes). The FE-prediction results included in the figure, which are in fact obtained by taking $k' = 0{\cdot}77$, are also close to the analytic solution. At lower Reynolds numbers the viscous region is physically larger of course, but the influence of the finite width of the plate increases, so that at $\mathrm{Re} = 10$ no region similar to the classic stagnation-point flow was predicted.

Whilst it is clearly possible to obtain good resolution of the viscous layer at $\mathrm{Re} = 100$ with a very fine grid, it is obvious that totally impracticable gridding would be required at the much higher Reynolds numbers associated with a turbulent wake flow. It is therefore important to determine whether good resolution of the viscous boundary layer is in fact necessary in order to obtain accurate predictions downstream of the fence. To this end, we considered the predictions of the flow in the region of the fence tip, where the boundary layer separates.

Figure 7 shows predictions of the velocity vector along $y/h = 1$, for $-1 \leq x/h \leq 0$, that is through the separating boundary layer. The flow angle results [Figure 7(a)] are all very similar, which implies that the streamline *directions* are reasonably predicted even for the FD solutions on a coarser grid (grid 1). However, FD predictions of the velocity magnitudes (both components) are rather lower than the FE results. Indeed, the grid 1 VDS and HDS solutions in Figure 7(b) show that the maximum total kinetic energy $((u^2+v^2)/u_0^2)$, which presumably is found at the edge of the separating boundary layer, is about 25 per cent less than that given by the FE calculation. An increased resolution near the fence, as in results for grid 3 shown in Figure 7(b), significantly reduces this difference.

Now we expect that any increase in the energy available in the separated shear layer will increase the distance to the point of reattachment, provided that the flow angles along, say, $y/h = 1$, $x < 0$, (or $x = 0$, $y/h > 1$) are identical. Thus the FE solution predicted reattachment

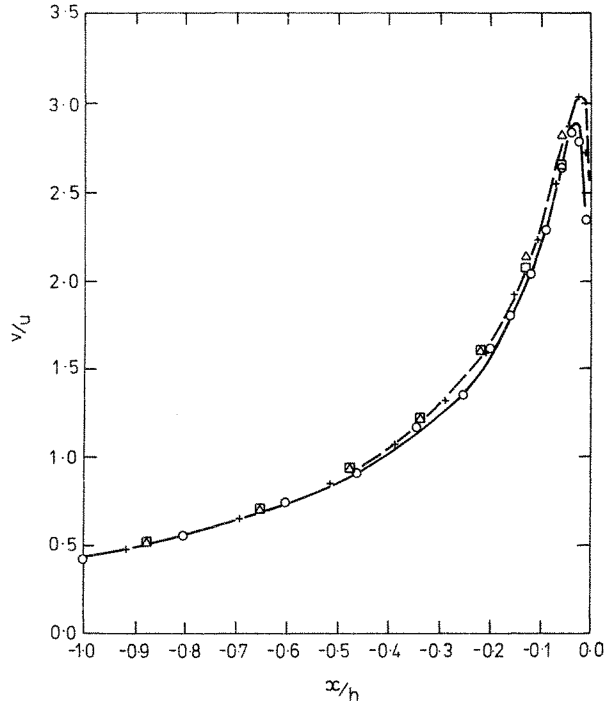

Figure 7(a). Direction of velocity vector (v/u) upstream of fence tip, $y/h = 1{\cdot}0$; $\mathrm{Re} = 100$. □, HDS Grid 1; △, VDS Grid 1; +, VDS Grid 3; ○, FE

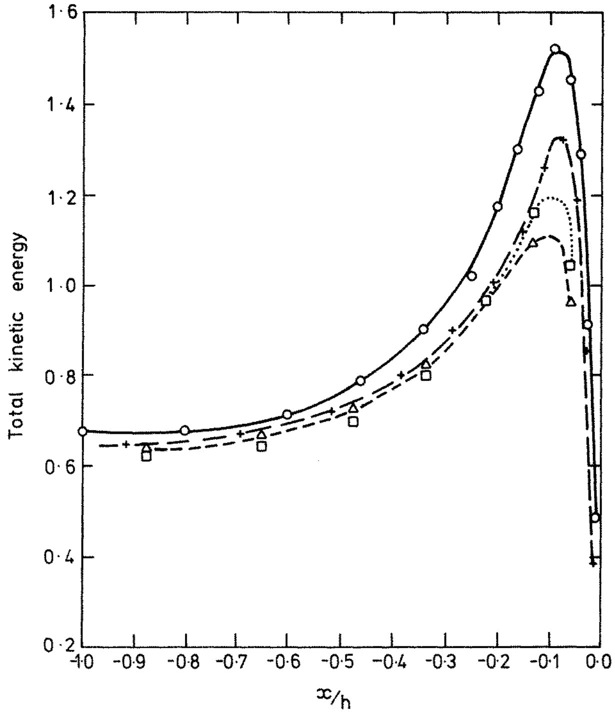

Figure 7(b). Total kinetic energy ($(v^2+u^2)/v_0^2$) upstream of fence tip. Legend as in Figure 7(a)

at about $x/h=25$, compared with VDS predictions of $x/h \simeq 20$. Now some of this difference may be due to errors in the VDS solution downstream of the plate; indeed the grid 3 VDS solution shown in Figure 7 actually gave a slightly smaller value of L/h than the corresponding grid 1 solution. However, this was almost certainly because grid 3 uses a coarser grid downstream to admit a finer resolution near the plate itself (see Section 4.2 for a more detailed discussion). Despite these complicating factors, the evidence indicates that good resolution of the flow near the fence is necessary for an accurate prediction of the high velocities that occur near separaiton. Figure 8 emphasizes this point: here the previous VDS-grid 1 solution for $y/h=1$ and $x<0$ is compared with results obtained from VDS predictions using coarser y-meshes (but the same x-mesh). Interestingly, the total kinetic energy near separation is actually *increased* as the grid becomes coarser [Figure 8(b)], but the flow angle is drastically reduced [Figure 8(a)], so that reattachment occurred rather earlier: L/h was about 15 per cent lower than the grid-1 prediction in the worst case. Although the results will not be presented here, comparisons between the various predictions for conditions along $x/h=0$, $y/h>1$ lead to very similar conclusions

4.2. *The separated shear layer*

Figure 9 shows the growth of the shear layer, plotted in the form suggested in Section 2.3, for $30 \leq \mathrm{Re} \leq 100$. The shear-layer thickness, δ_l, was defined as the distance between those points where the axial velocity exceeds $u_{\min}$ by 0·05 and 0·95 times the value of $(u_{\max}-u_{\min})$ at that value of x; $u_{\min}$ was of course negative since the shear layer bounds a recirculating region.

In studying the behaviour of predictions of the separated shear layer, all finite-difference

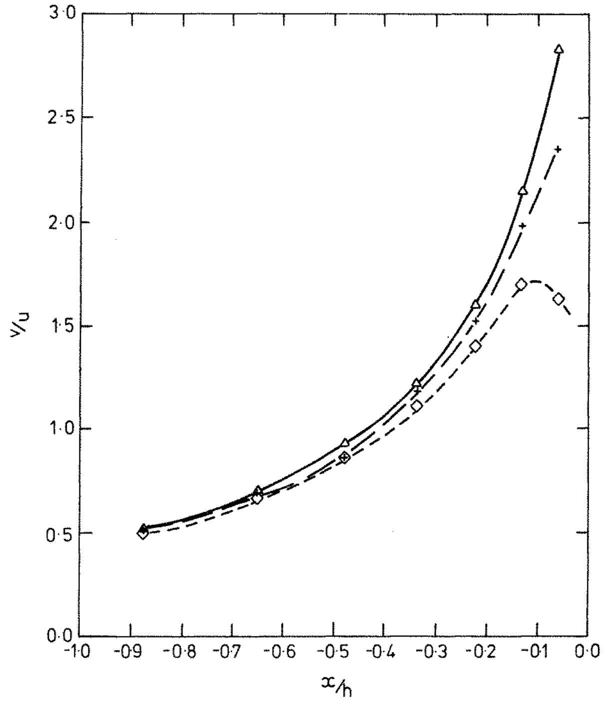

Figure 8(a). Dependence on velocity direction upstream of fence tip on y-grid refinement. VDS Grid 1 in x-direction, $Re = 100$. △, standard Grid 1 y-mesh with $\Delta y/h = 0{\cdot}014$ at fence tip; +, $\Delta y/h = 0{\cdot}04$; ◇, $\Delta y/h = 0{\cdot}20$

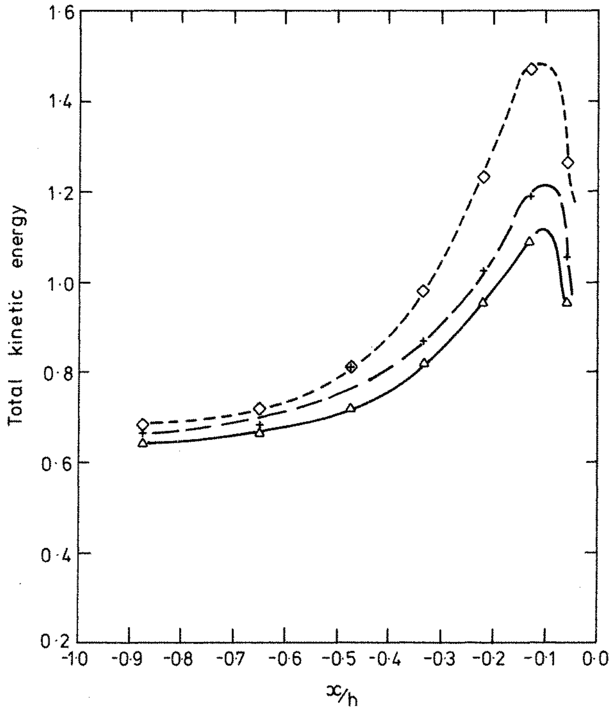

Figure 8(b). Dependence of kinetic energy on y-grid refinement. Legend as in Figure 8(a)

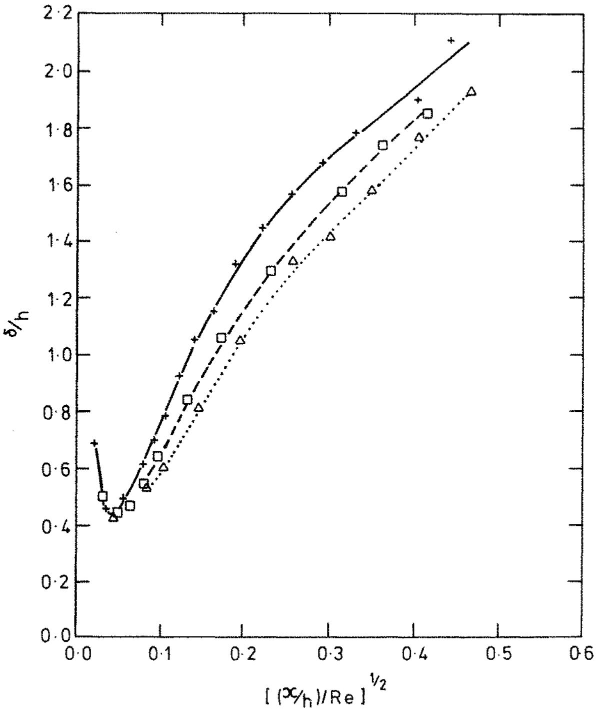

Figure 9(a). Shear layer growth, HDS. Re = : △, 30; □, 50; ○, 70; +, 100

results presented in this section were obtained using grid 1. Resolution of the boundary layer at separation is not really adequate (see previous section), but this grid is finer in the separated region than grid-3; we believe that it is therefore a suitable compromise.

The HDS results at different Reynolds number, which are shown in Figure 9(a), do not coincide even in the region where the axial pressure gradient is roughly zero ($[(x/h)/\mathrm{Re}]^{1/2} \leq$ 0·25). They also predict both a thicker shear layer (at a given x) and a greater rate of growth at higher Reynolds numbers. This is symptomatic of numerical diffusion and leads to early reattachment (see Section 4.3). In contrast, the VDS results in Figure 9(b) coincide at all Reynolds numbers in the range under study, except that the results at Re = 100 are distinct in the region of positive pressure gradient. It is probably unrealistic to look for much significance in this latter observation, because it is difficult to analyse the development of the shear layer in the region where the layer is perturbed by the influence of the upper boundary and the splitter plate.

The FE results for different Reynolds numbers, which are shown in Figure 9(c), also coincide to reasonable accuracy. These predictions were obtained using the grid in Table II at Re = 100, but with the downstream grid compressed at lower Reynolds number to maintain a constant number of nodes in the recirculating region. The FE grid is in fact finer than the grid-1 used for the FD calculations at all Reynolds numbers, but FE predictions with any coarser grid has irregular streamlines. This difference in the grids may explain the rather unexpected results seen in Figure 9(d), which shows the various predictions of shear-layer growth at Re = 100: the FE calculation predicts a greater thickness for the shear layer than the VDS. The reason for this is not clear: numerical diffusion will usually, and always with standard hybrid differencing, lead to too rapid a growth of regions of high

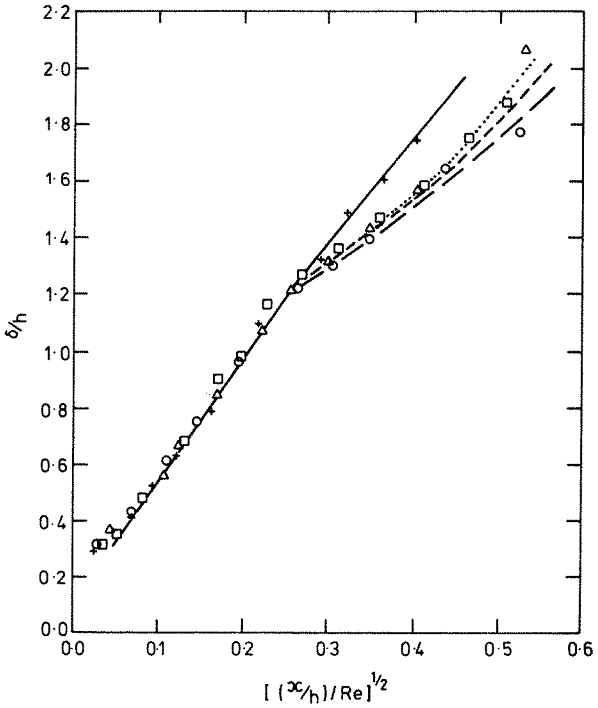

Figure 9(b). Shear layer growth, VDS, Legend as in Figure 9(a)

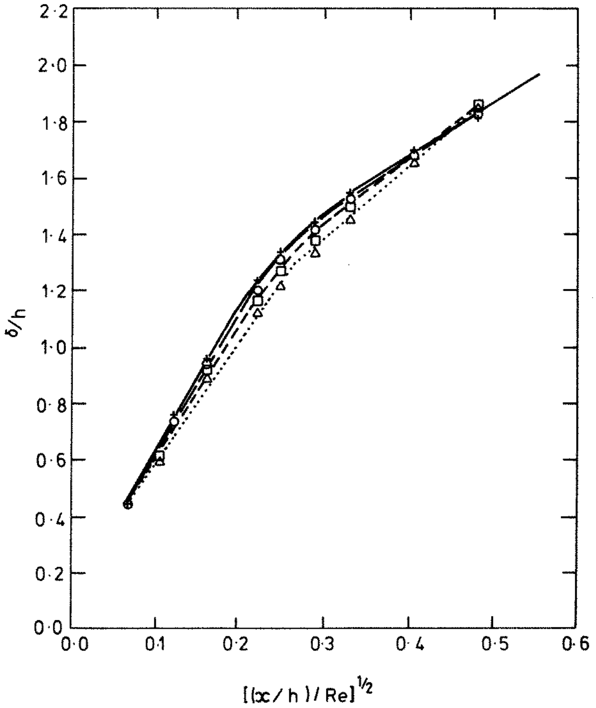

Figure 9(c). Shear layer growth, FE. Legend as in Figure 9(a)

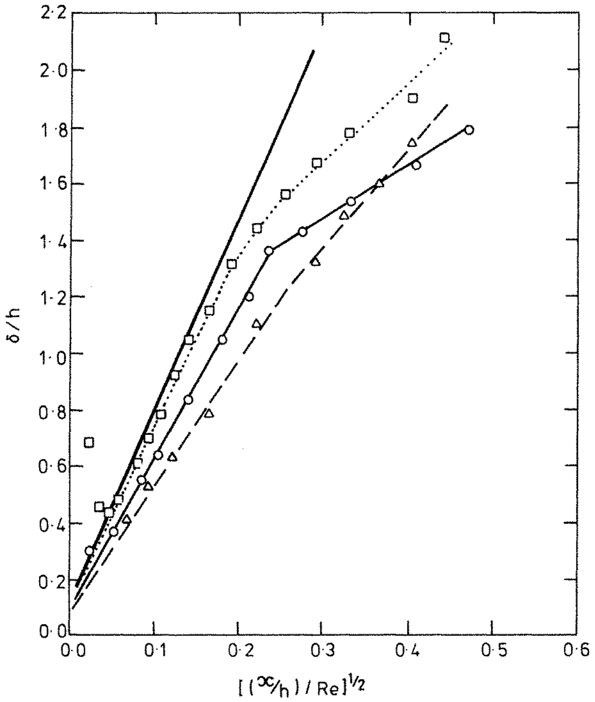

Figure 9(d). Shear layer growth, Re = 100. □, HDS: △, VDS; ○, FE;———Lock's analytic solution for plane mixing layer

vorticity if the mesh Reynolds numbers exceed two; it is difficult to see how vector differencing could lead to the opposite result. However, the shear layer in the FE calculation is more energetic and more strongly deflected than in the VDS prediction; thus a simple comparison of the rate of shear-layer growth may be unrealistic if the different shear layers do not develop in comparable conditions but, for example, in varying pressure gradients.

Lock's[41] solution for the classical plane mixing layer was used to calculate the growth of the 0·05–0·95 thickness, and this result is included in Figure 9(d). In view of the preceding remarks, we believe that the close agreement between the HDS results at Re = 100 and the classic mixing layer is wholly fortuitous, and that the actual growth rate of the separated shear layer is a little lower than the latter. This is not surprising as the separated shear layer is subjected to a significant transverse pressure gradient during its initial development. it could be argued that this will tend to inhibit its growth, but not destroy the classic dependence on $(x/\mathrm{Re})^{1/2}$, since this transverse gradient is, initially at least, fairly constant with x.

4.3. Surface pressures and bubble length

Figure 10 shows various predictions of the surface-pressure coefficient, C_p, defined as

$$C_p = (p - p_0)/\tfrac{1}{2}\rho u_0^2, \tag{18}$$

where p is the pressure on the splitter plate and u_0 and p_0 are field values at the inlet. The pressure coefficient is plotted against $(x/h)/\mathrm{Re}$ because as indicated in Section 2.3, flow variations in the axial direction are expected to scale linearly with Reynolds number at sufficiently high values of Re. However, we cannot expect a relation of this form to persist

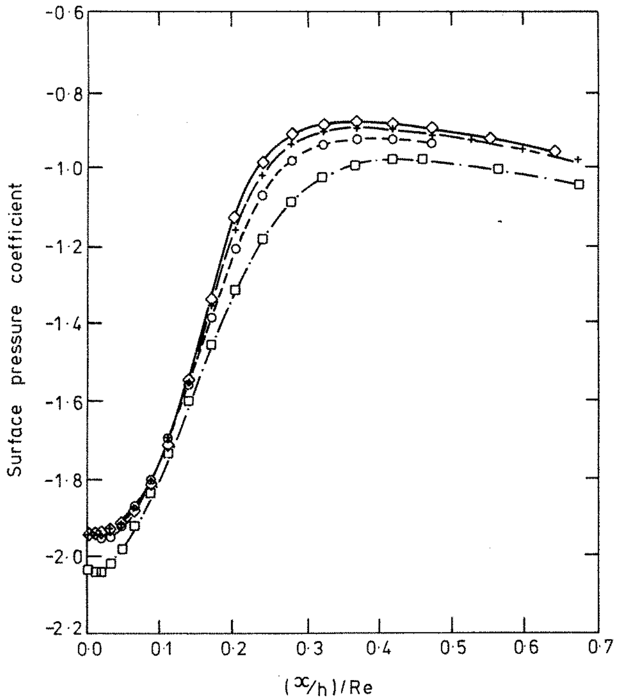

Figure 10(a). Surface pressure coefficients. VDS, Re = : △, 20; □, 30; ○, 50; +, 70; ◇, 100

down to Reynolds numbers at which the shear-layer growth still maintains the dependence on $\mathrm{Re}^{1/2}$ found at high Reynolds number.

The VDS results indeed collapse only for $R \geq 50$ [Figure 10(a)] while it can be seen in Figures 9(b) and 9(c) that calculations of shear-layer growth scale accurately with $\mathrm{Re}^{1/2}$ at least down to $\mathrm{Re} = 30$. The FE results (not shown) have a similar behaviour but, in contrast, the HDS calculations of the pressure coefficient show a significantly greater spread. Figure 10(b) shows predictions for $\mathrm{Re} = 100$ obtained using the three numerical methods; clearly the FE method gives the slowest and the HDS the most rapid pressure recovery. Note also that the base pressure is significantly lower for the FE prediction; this is precisely what would be expected from the results presented in Section 4.1, where it was seen that the separating boundary layer was significantly more energetic for the FE prediction. The trend in the results shown in Figure 10(b) is not the same as that observed in 9(d), but, as argued earlier, the pressure recovery—and the distance to reattachment—are *not* determined solely by the growth of the shear-layer thickness. It was pointed out in Section 4.1 that the magnitude and direction of the flow around separation are also likely to be important in determining the downstream flow; recall that grid 1 was used for the finite-difference predictions of Figures 9 and 10, whereas an even finer grid (near the fence) was required to obtain details of the separating boundary layer close to those given by the FE method (Section 4.1).

Figure 11 is a plot of the fence surface-pressure coefficients for $\mathrm{Re} = 100$, predicted using VDS and HDS with grid 1, VDS with grid 3, and the standard FE grid in Table II. There is a very rapid fall in pressure on the front of the fence as $y/h \to 1$, and clearly the finite-difference solutions on a coarser grid tend to smooth out the rapid changes predicted in the FE solution. VDS with grid 3 is better in this respect, as expected. Since staggered grids have to be used for the finite-difference methods, the difference procedures used in the region

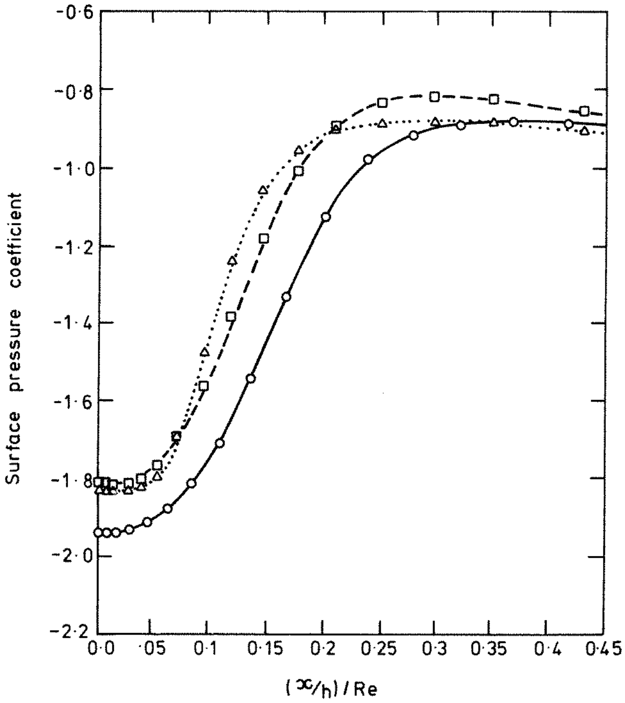

Figure 10(b). Surface pressure coefficients. △, HDS; □, VDS; ○, FE

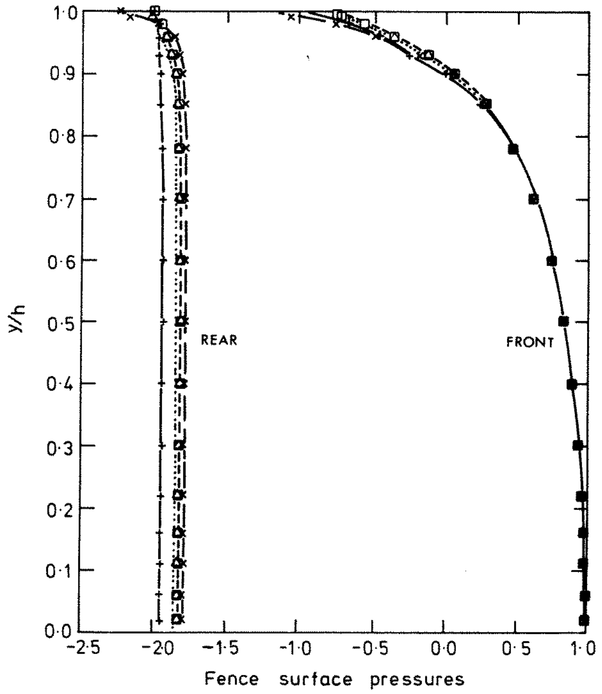

Figure 11. Fence surface pressures. Re = 100. △, HDS Grid 1; □, VDS Grid 1; ×, VDS Grid 3; +, FE

surrounding the fence tip must be defined with great care—the details differ for each variable and will not be discussed here. There is an increasingly large discontinuity in the pressure gradient along, say, $y/h=1$ at $x/h=0$ as Re increases; this is associated of course with the fact that v/u must tend to infinity (as $\mathrm{Re}\rightarrow\infty$) just outside the viscous boundary layer at separation. It is clear that increasingly fine grids would be required to resolve this region of the flow as Re increases; presumably the necessary resolution should scale roughly with $\mathrm{Re}^{1/2}$. The implications of this for computation of the corresponding high Reynolds-number turbulent flow are discussed later.

The final results of the various predictions are given in Figure 12, where the normalized distance to reattachment, L/h, of the separated shear layer is plotted for the VDS and HDS grid 1, and standard FE solutions. It is clear that differences between the various solutions increase with Reynolds number. In particular, hybrid differencing does not lead to a linear growth of L with Re, as originally anticipated, and as the previous results would suggest; VDS solutions, however, do exhibit the expected behaviour, although the predicted L/Re is not as high as that given by the FE calculations. In view of the results discussed in Section 4.1, we believe that this must be due almost entirely to inadequate resolution near the plate. Since in the VDS solutions, the downstream surface pressures and shear-layer growth rate have the expected behaviour for $\mathrm{Re}\gtrsim 30$, it is difficult to explain too low a value of L/Re on grid deficiencies downstream of the plate. The one case where grid resolution near the fence was improved (VDS, Re = 100, grid 3) had a rather coarser grid downstream (limited by the maximum allowable number of grid nodes), and consequently the prediction did not show a larger L/h. A further increase in the number of grid nodes in the axial direction to allow finer resolution near the plate without grid degradation elsewhere, would, we believe, increase the

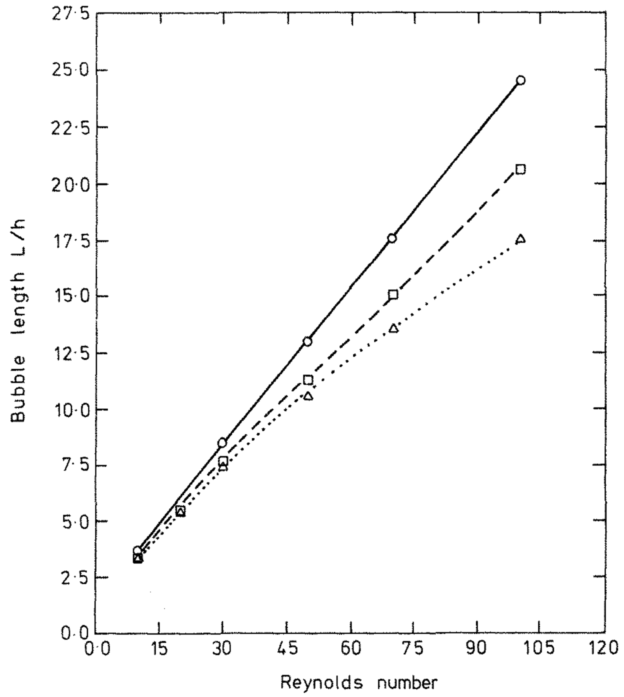

Figure 12. Variation of bubble length with Reynolds number. △, HDS; □, VDS; ○, FE

slope of the L vs. Re predictions for VDS, but would not change the basic difference between the HDS and VDS solutions.

5. DISCUSSION AND CONCLUSIONS

We have seen that the nature and significance of the errors in our calculations depend first on the particular numerical method, but also on the region of the flow where each method is employed. In the irrotational region upstream of the boundary layer on the front of the plate, there is a balance between pressure gradients, which enter the equations of fluid flow as source terms, and the inertial forces, which introduce convective terms. In this region the two finite-difference schemes are inaccurate because they do not conserve energy, and the resulting errors in the predicted flow may subsequently be convected downstream of the barrier. The finite-element method, on the contrary, does not invoke upwinding and is more nearly akin to a central-difference scheme; it therefore behaves more satisfactorily in the irrotational region because the integrals of motion, in particular the kinetic energy, are more nearly conserved. The penalty to pay for this advantage is that it is necessary to use a refined grid that resolves the boundary layer; otherwise, the solution of the flow equations is beset with wiggles.

We have remarked that laminar flow over a plate at $\mathrm{Re}=O(100)$ is qualitatively similar to turbulent flow at high Reynolds number, so that the irrotational flows in the two cases must correspond. Even if there is turbulence in the upstream flow, the flow equations have the same dominant terms, which require for their accurate solution a numerical scheme that conserves energy. However, it is then still necessary to resolve the much thinner boundary layer at high Reynolds numbers with a very fine grid, in order to avoid oscillatory solutions. On the other hand, schemes like HDS and VDS maintain stability by introducing dissipation into their description of the convective terms in the flow equations; it is not then essential to resolve the boundary layer. But such methods, as we have seen, introduce significant errors in the irrotational region, principally associated with energy loss from the flow. However, such errors are bounded and may not be much larger for $\mathrm{Re}=O(10^5)$ than they are in the present case (Figure 5)—they could be reduced by refining the grid. Our results show that flow around separation, which is important in determining the characteristics of the downstream flow, can be predicted with acceptable accuracy using such methods, provided that the grid *near the plate* is sufficiently fine—it seems more important to resolve the flow in the regions of rapid gradients just outside the boundary layer (e.g. $-1<x/h<0$, Figure 7) than further upstream where mesh Reynolds numbers are actually higher. An adequate grid must have mesh spacings no larger than a few per cent of the plate height in that region. This may not resolve the boundary layer at high Reynolds number, but is sufficient for reasonably accurate prediction of the potential flow around separation.

The characteristics of the flow in the downstream region are quite different: pressure gradients have less significance and the equations of motion impose a balance between viscous and inertial forces, particularly in the shear layer. In fact these differences in the basic character of the flow preclude the choice of a single numerical method that is ideal both in front and behind the barrier. In assessing the performance in the downstream region of the various methods considered in this paper, we find that HDS is certainly inadequate in comparison with the higher-order schemes. The simple upwinding technique in the hybrid scheme introduces numerical diffusion that leads to a too rapid spread of vorticity, and as a result to premature reattachment of the separated shear layer. Since the recirculation regions are very similar in size for $\mathrm{Re}=O(100)$ and $\mathrm{Re}=O(10^5)$, we would expect to find similar numerical errors, so that simple low-order schemes like HDS will not be very satisfactory for calculations of turbulent flow at high Reynolds numbers. A major conclusion of this work is that such schemes should be used with great caution.

We cannot, of course, infer conversely that the VDS or FE methods, which seem to be adequate for predicting laminar flows, will also perform well in studies of turbulent flow. (Indeed, as noted earlier, the latter requires resolution of the boundary layer on the front of the plate, so would probably be impossible to apply directly in a $\mathrm{Re}=10^5$ situation). The equations of the various presently favoured models of turbulence are more complex and involve additional equations representing, for example, transport of turbulence kinetic energy or shear stress. The stability of the several equations therefore depends not only on their separate representation in difference form, but also on the non-linear coupling between the various variables. Despite this uncertainty, we believe there is a need to seek for a more accurate and robust numerical method, which can be applied with confidence to flows that have distinct regions with quite different characteristics. Such a method must involve a compromise between enhancing stability and minimizing numerical diffusion. The promising approach of Hughes and Brooks[42] uses different discretizations of the bulk of the flow and the 'boundary layer' regions; theirs was a finite-element method, but the idea could be used with finite differences. However, there is an immediate opportunity to apply even the simplest higher-order schemes like VDS, or for example, the relatively straightforward third-order method of Leonard,[35] to calculations of turbulent flow.

Finally, we should emphasize that we have not overtly sought for a definitive solution for laminar flow over a flat plate. The particular flow geometry, and the numerical methods used to solve this problem, have been chosen rather to highlight difficulties that will also arise in calculations of complex flow at high Reynolds number using those methods now in common use. Nevertheless, the finite-element solution seems to be reasonably accurate and we look forward to comparing these results with experimental data when they become available.

ACKNOWLEDGEMENTS

This work was begun while one of the authors (IPC) was employed at the Marchwood Engineering Laboratory of the Central Electricity Generating Board, and is published by permission of its Director. The same author is also grateful to the US Environmental Protection Agency, who funded his appointment as Visiting Assistant Professor in the Department of Geosciences, NC State University, during which time a first draft of this paper was prepared.

REFERENCES

1. S. E. Pope and J. H. Whitelaw, *J. Fluid Mech.* **73,** 9 (1976).
2. L. J. S. Bradbury, F. Durst, B. E. Launder, F. W. Schmidt and J. H. Whitelaw, (Ed.), *Turbulent Shear Flows 2,* Springer-Verlag, Berlin, 1980.
3. B. P. Leonard, M. A. Leschziner, and J. McGuirk, in *Numerical Methods in Laminar and Turbulent Flows* Eds. C. Taylor, K. Morgan and C. A. Brebbia, Pentech, London 1978, p. 807.
4. D. B. Spalding, *Int. J. num. Meth. Engng,* **4,** 551 (1972).
5. A. D. Gosman, W. M. Pun, A. K. Runchal, D. B. Spalding and M. Wolfshtein, in *Heat and Mass Transfer in Recirculating Flows,* Academic Press, New York, 1969.
6. C. W. Hirt, *J. Comput. Phys.* **2,** 339 (1968).
7. Sin-I. Cheng, *Phys. Fluids Supp.,* **12,** 34 (1969).
8. P. J. Roache, *Computational Fluid Dynamics,* Hermosa, Albuqerque, 1972.
9. A. G. Hutton, in *Numerical Methods in Applied Fluid Dynamics* (Ed. B. Hunt), Academic Press, New York, 1980, p. 177.
10. G. D. Raithby, *Comp. Meth. in App. Mech. and Engng,* **9,** 153 (1976).
11. I. P. Castro, in *Numerical Methods in Laminar and Turbulent Flow* (Eds. C. Taylor, K. Morgan and C. A. Brebbia), Pentech, London, 1978, p. 329.
12. J. N. Lillington, *Int. j. Numer. methods fluids,* **1,** 3–16 (1981).

13. B. P. Leonard, in *Computational Techniques for Transient and Turbulent Flow* (Ed. C. Taylor and K. Morgan), Pineridge Press, Swansea, 1981.
14. P. M. Gresho and R. L. Lee, *Computers and Fluids* **9,** 223 (1981).
15. C. Taylor and P. Hood, *Computers and Fluids,* **1,** 73 (1973).
16. C. Taylor and P. Hood, in 'Finite element methods in flow problems', *Proc. First Int. Symp.* (Ed. J. T. Oden, O. C. Zienkiewicz, R. H. Gallagher and C. Taylor), UAH Press, Huntsville, Alabama, 1974, p. 121.
17. M. Kawahara, N. Yoshimuar and K. Nakagawa. in 'Finite element methods in flow problems', *Proc. First Int. Symp.* (Ed. J. T. Oden *et al.*), UAH Press, Huntsville, Alabama, 1974, p. 107.
18. R. M. Smith, *CEGB Rep. RD/B/N*3513 (1975).
19. A. G. Hutton and R. M. Smith, *CEGB Report RD/B/N*3660 (1979).
20. K. H. Winters and K. A. Cliffe, *AERE Harwell Report R.*9444 (1979).
21. R. M. Smith and A. G. Hutton, *CEGB-BNL Memorandum, BM/PS/*004 (1977).
22. M. Bercovier and O. Pironneau, *Numer. Math.* **33,** 211 (1979).
23. P. LeTallec, *Numer. Math.* **35,** 381 (1980).
24. J. J. McGuirk and W. Rodi, *J. Fluid Mech.* **86,** 761 (1978).
25. M. Arie and H. Rouse, *J. Fluid Mech.,* **1,** 129 (1956).
26. C. Chandrsuda and P. Bradshaw, *J. Fluid Mech.,* to appear (1981).
27. H. H. Schlichting, *Boundary Layer Theory,* McGraw-Hill, New York, 1968.
28. S. V. Patankar and D. B. Spalding, *Int. J. Heat and Mass Transfer,* **15,** 1787 (1972).
29. J. E. Fromm and F. H. Harlow, *Phys. Fluids,* **6,** 975 (1963).
30. D. K. Lilly, *Mon. Wea. Rev.,* **93,** 11 (1965).
31. J. W. Deardorff, *J. Fluid Mech.,* **41,** 453 (1970).
32. D. N. Allen and R. V. Southwell, *Quart. J. Mech. and App. Math.* **8,** 129 (1955).
33. G. D. Raithby and K. E. Torrance, *Computers and Fluids,* **2,** 191 (1974).
34. I. P. Castro, in *Turbulent Shear Flows* 1 (Eds. F. Durst and B. E. Launder) (1979).
35. B. P. Leonard, *Comp. Meth. in App. Mech. and Engng,* **19,** 59 (1979).
36. C. P. Jackson and K. A. Cliffe, 'The necessity for mixed interpolation in primitive variable formulations of the Navier–Stokes equations', *Int. J. num. Meth. Engng,* to appear (1982).
37. R. L. Sani, P. M. Gresho, R. L. Lee and D. F. Griffiths, *Int. j. numer. methods fluids,* **1,** 17 (1981).
38. O. C. Zienkiewicz, *The Finite Element Method in Engineering Science,* McGraw-Hill, New York, 1977.
39. P. Hood, *Int. j. num. Meth. Engng,* **10,** 379 (1976).
40. G. V. Parkinson and T. Jandali, *J. Fluid Mech.,* **40,** 577 (1970).
41. R. C. Lock, *Quart. J. mech. and App. Math.,* **4,** 42 (1955).
42. T. J. R. Hughes and A. Brooks, in *Boundary and Interior Layers—Computational and Asymptotic Methods* (Ed. J. J. H. Miller), Boole, Dublin, 1980, p. 103.